Effective Polyakov line action from the relative weights method

Jeff Greensite and Kurt Langfeld

Effective Polyakov line action from the relative weights method

Jeff Greensite

Niels Bohr International Academy, Blegdamsvej 17, DK-2100 Copenhagen Ø, Denmark[*]

Kurt Langfeld

School of Computing & Mathematics,
University of Plymouth, Plymouth, PL4 8AA, UK

Abstract

We apply the relative weights method (arXiv:1209.5697) to determine the effective Polyakov line action for SU(2) lattice gauge theory in the confined phase, at lattice coupling $\beta = 2.2$ and $N_t = 4$ lattice spacings in the time direction. The effective action turns out to be bilinear in the fundamental representation Polyakov line variables, with a rather simple expression for the finite range kernel. The validity of this action is tested by computing Polyakov line correlators, via Monte Carlo simulation, in both the effective action and the underlying lattice theory. It is found that the correlators in each theory are in very close agreement.

---

[*] Permanent address: Physics and Astronomy Dept., San Francisco State University, San Francisco, CA 94132, USA

I. INTRODUCTION

The Polyakov line action (PLA) is an action obtained from lattice gauge theory when all degrees of freedom are integrated out, under the constraint that the Polyakov line holonomies are held fixed. There are some indications [1–4] that the sign problem in this theory, at non-zero chemical potential, may be more tractable than the sign problem in the underlying lattice gauge theory (for a review, cf. [5]), and if so it could provide us with a new tool for investigating the QCD phase diagram. It is fairly straightforward, given the PLA at chemical potential $\mu = 0$, to introduce a non-zero chemical potential, as we discuss in section V. The problem we address here is how to extract the PLA from the underlying lattice gauge theory at $\mu = 0$.

This article is a follow-up to ref. [6], which presented a novel "relative weights" technique for deriving the PLA, based on a method used previously in studies of the Yang-Mills vacuum wavefunctional [7]. The method was tested at strong couplings, where the answer is known, and a conjecture for the action at a weaker coupling, for SU(2) pure gauge theory at $\beta = 2.2$ and inverse temperature $N_t = 4$ lattice spacings, was presented. This conjecture was based, however, on a study limited to fairly atypical regions of field configuration space. Below we will apply the method in the region expected to dominate the path integral, and a rather different (and in fact simpler) action from the one conjectured in ref. [6] emerges. As a crucial test of the derived PLA, we compute the two-point Polyakov line correlator from Monte Carlo simulations of both the PLA and the underlying gauge theory. These correlators will be seen to agree quite accurately. Our effective PLA turns out to be only bilinear in the Polyakov line variables, with a simple expression for the finite range kernel.

There have been a number of previous attempts to derive the PLA from lattice gauge theory at finite temperature. These include strong-coupling expansions [2], the Inverse Monte Carlo method [8], and the demon approach [9]. All of these methods generate effective Polyakov line actions of varying degrees of complexity. We believe, however, that an accurate agreement of Polyakov line correlators in the confined phase, computed in the effective and underlying lattice gauge theories, has not been demonstrated in any of the previous studies, at least not beyond two or three lattice spacings in Polyakov line separation.

It should also be mentioned that there are a number of studies which are concerned with deducing the Polyakov line potential, with particular application to the deconfinement transition, c.f. [10] and references therein. There have also been efforts, e.g. [11], to express the fermion determinant in terms of a potential involving Polyakov lines. These studies do not arrive at a full PLA as defined above, and hence their focus is somewhat different from ours.

Our article is organized as follows: An improved version of the relative weights method is presented in section II below. The technique is applied to pure SU(2) gauge theory in section III, again at $\beta = 2.2$ and $N_t = 4$, and the Polyakov line correlators of the derived PLA are compared to those of lattice gauge theory. Application to a gauge-Higgs theory, with a scalar matter field explicitly breaking global Z_2 center symmetry, is presented in section IV. Section VI contains our conclusions. The extension of our method to gauge theories with dynamical fermions is discussed in an appendix.

II. THE RELATIVE WEIGHTS METHOD

The relative weights method, as applied to deriving the PLA S_P, was introduced in ref. [6]. The technique is particularly well adapted to computing path (or "directional") derivatives of the effective action S_P in the space of all Polyakov line configurations. A single configuration $\{U_{\boldsymbol{x}}\}$

is a point in this space, where we specify the group-valued Polyakov line holonomies $U_{\boldsymbol{x}}$ at each spatial point $\boldsymbol{x}$ in a three-dimensional volume. Let $\{U_{\boldsymbol{x}}(\lambda)\}$ be a path through this space of configurations, where λ parametrizes the path. The relative weights method computes the path derivative $\partial S_P[U_{\boldsymbol{x}}(\lambda)]/\partial\lambda$ at some given $\lambda = \lambda_0$. In this section we present a variant of the relative weights approach which, while equivalent to the original method of [6], is numerically more efficient.

In order to minimize minus signs later on, we adopt the convention that the Boltzmann weight is proportional to $\exp[+S_P]$. Let S_L be the lattice gauge action on an $L^3 \times N_t$ volume with coupling β for the Wilson action. S_L may contain pseudofermion or bosonic matter degrees of freedom, collectively denoted by ϕ. It is convenient to go to temporal gauge, so that all timelike link variables are set to the unit matrix except on a timeslice at $t = 0$. Then the PLA S_P is defined as

$$\exp\left[S_P[U_{\boldsymbol{x}}]\right] = \int DU_0(\boldsymbol{x},0)DU_k D\phi \left\{\prod_{\boldsymbol{x}} \delta[U_{\boldsymbol{x}} - U_0(\boldsymbol{x},0)]\right\} e^{S_L} . \tag{1}$$

Because of the residual $U_0(\boldsymbol{x},0) \to g(\boldsymbol{x})U_0(\boldsymbol{x},0)g^\dagger(\boldsymbol{x})$ symmetry in temporal gauge, it follows that S_P can only depend on the eigenvalues of the $U_{\boldsymbol{x}}$ matrices.

While the functional integration in (1) can only be carried out in special cases, e.g. via strong coupling and hopping parameter expansions valid a certain range of parameters, the ratio (or "relative weights") $\exp[S_P[U'_{\boldsymbol{x}}]]/\exp[S_P[U''_{\boldsymbol{x}}]]$ evaluated at nearby configurations $U'_{\boldsymbol{x}}$, $U''_{\boldsymbol{x}}$ is calculable numerically. This fact enables us to compute path derivatives of S_P.

Let us consider a set of M Polyakov line configurations

$$\left\{\{U_{\boldsymbol{x}}^{(n)}, \text{all } \boldsymbol{x}\}, \ n = 1,2,...,M\right\} , \tag{2}$$

corresponding to values of the path parameter

$$\lambda_n = \lambda_0 + \left(n - \frac{M+1}{2}\right)\Delta\lambda \ , \quad n = 1,2,...,M \quad , \tag{3}$$

and define

$$S_L^{(m)}[U,\phi] \equiv S_L\left[U_0(\boldsymbol{x},0) = U_{\boldsymbol{x}}^{(m)}, U_k(x,t), \phi(x,t)\right] \tag{4}$$

to be the lattice action in temporal gauge with the timelike links at $t = 0$ fixed to the m-th member of the set (2). We also define

$$\Delta S_P^{(m+1)} \equiv S_P[U^{(m+1)}] - S_P[U^{(m)}]$$

$$Z_m \equiv \int DU_k D\phi \ e^{S_L^{(m)}} . \tag{5}$$

3

From (1), we have

$$
\begin{aligned}
\exp[\Delta S_P^{(m+1)}] &= \frac{\exp\left[S_P[U^{(m+1)}]\right]}{\exp\left[S_P[U^{(m)}]\right]} \\
&= \frac{\int DU_k D\phi \ e^{S_L^{(m+1)}}}{\int DU_k D\phi \ e^{S_L^{(m)}}} \\
&= \frac{\int DU_k D\phi \ \exp\left[S_L^{(m+1)} - S_L^{(m)}\right] e^{S_L^{(m)}}}{\int DU_k D\phi \ e^{S_L^{(m)}}} \\
&= \left\langle \exp\left[\Delta S^{(m+1)}\right] \right\rangle_m ,
\end{aligned}
\tag{6}
$$

where $\langle...\rangle_m$ indicates that the expectation value is taken from ensembles with Boltzmann factor $\exp[S^{(m)}]/Z_m$. For sufficiently small $\Delta\lambda$,

$$
\begin{aligned}
\frac{dS_P[U_{\boldsymbol{x}}(\lambda)]}{d\lambda} &\approx \frac{\Delta S_P^{(m+1)}}{\Delta\lambda} \\
&= \frac{1}{\Delta\lambda} \log\left(\left\langle \exp\left[\Delta S^{(m+1)}\right]\right\rangle_m\right) ,
\end{aligned}
\tag{7}
$$

Derivatives evaluated at each m should, in principle, be very nearly the same for small enough $\Delta\lambda$, and should closely agree, for all $m < M$, with the derivative evaluated at the central value of $\lambda = \lambda_0$. The main source of error is not the discretization of the derivative (which could be reduced by using a central or multi-point approximation), but rather the ordinary statistical error in computing (6) via lattice Monte Carlo. We can then improve our estimate of the derivative by making use of all M configurations, and taking the average

$$
\left(\frac{dS_P[U_{\boldsymbol{x}}(\lambda)]}{d\lambda}\right)_{\lambda=\lambda_0} \approx \frac{1}{\Delta\lambda} \frac{1}{M-1} \sum_{m=1}^{M-1} \log\left(\left\langle \exp\left[\Delta S^{(m+1)}\right]\right\rangle_m\right) .
\tag{8}
$$

In practice we have found that this procedure results in a considerable reduction in the error of $dS_p/d\lambda$, as compared to our previous implementation of the relative weights method in ref. [6].

The question then becomes which point $\{U_{\boldsymbol{x}}(\lambda_0)\}$ in configuration space should be chosen for the computation, and which directional derivatives $dS_P/d\lambda$ at this point should computed, in order to deduce S_P. It is possible that the choice is not very important, and that S_P is well approximated by the same simple expression everywhere in configuration space. However, if this is not the case, then calculating path derivatives in some very atypical corner of configuration space may lead to an approximate answer for S_P which may be correct in that particular corner, but misleading in the bulk of configuration space.

In ref. [6] the path derivatives were computed using three types of sets (2) for SU(2) lattice gauge theory. These were (i) Polyakov lines which were constant in space, and the λ parameter was the amplitude of $P_{\boldsymbol{x}} = \frac{1}{2}\text{Tr}[U_{\boldsymbol{x}}] = \lambda$; (ii) Polyakov lines which consisted of small plane wave fluctuations around a constant background, $P_{\boldsymbol{x}} = P_0 + \lambda \cos(\boldsymbol{k} \cdot \boldsymbol{x})$ with $\lambda \ll P_0$; and (iii) Polyakov lines in which $P_{\boldsymbol{x}}$ varied as $P_{\boldsymbol{x}} = \lambda \cos(\boldsymbol{k} \cdot \boldsymbol{x})$. Compared to thermalized timeslice configurations $U_0(\boldsymbol{x}, 0)$ generated in a normal lattice Monte Carlo simulation, such configurations are very atypical. In a thermalized configuration in the confined phase, the Fourier components of the

configuration are all of $O(1/\sqrt{V_3})$, where $V_3 = L^3$ is the lattice volume of the D=3 dimensional timeslice, whereas in the special configurations just mentioned, one Fourier component (which may be the zero mode) is of $O(1)$. For computing the PLA at a strong lattice coupling, where this action can be evaluated via a strong coupling expansion, the atypical nature of the constant + plane wave, or pure plane wave configurations did not seem important, and the PLA deduced from the relative weights data was a close match to the known result. There was no similar result to compare to at $\beta = 2.2$, $N_t = 4$, and although an expression for S_P matching the results for $dS_P/d\lambda$ was deduced from fitting the data, there is a concern that this expression might only be valid in the special region of configuration space where it was derived.

We will investigate the action in more typical regions of configuration space in the next section.

III. DERIVATIVES OF S_P IN A THERMALIZED BACKGROUND

The goal is to use the expression for the path derivative (8) to determine S_P. However, if S_P does not have a simple form everywhere in configuration space (and it may not), then it is at least required that we have a fairly accurate approximation to S_P in the region which is important for the computation of observables, i.e. the region occupied by typical thermalized configurations $\{U_x\}$. A set of timelike link configurations $\{U_0(\boldsymbol{x},0)\}$ on the $t = 0$ timeslice, generated by a numerical simulation of the underlying lattice gauge theory, is a sample of such configurations. Let us define, for the SU(2) gauge group that we will consider here,

$$P_{\boldsymbol{x}} \equiv \frac{1}{2}\text{Tr}[U_{\boldsymbol{x}}] = \frac{1}{2}\sum_{\boldsymbol{k}}\left\{a_{\boldsymbol{k}}\cos(\boldsymbol{k}\cdot\boldsymbol{x}) + b_{\boldsymbol{k}}\sin(\boldsymbol{k}\cdot\boldsymbol{x})\right\}, \tag{9}$$

where the sum runs over all wavevectors $\boldsymbol{k}$ on a cubic lattice of volume L^3, and $a_{\boldsymbol{k}} = a_{-\boldsymbol{k}}$, $b_{\boldsymbol{k}} = -b_{-\boldsymbol{k}}$ are real-valued. Then we may consider calculating numerically, by the relative weights method, derivatives with respect to the Fourier components

$$\left(\frac{\partial S_P}{\partial a_{\boldsymbol{k}}}\right)_{a_{\boldsymbol{k}}=\alpha} , \quad \left(\frac{\partial S_P}{\partial b_{\boldsymbol{k}}}\right)_{b_{\boldsymbol{k}}=\alpha} , \tag{10}$$

in a background in which all other Fourier components are drawn from a thermalized configuration. By calculating the derivative for some range of α, it is possible to extrapolate to small α of order $1/\sqrt{V_3}$, which is the typical magnitude of a Fourier component in thermalized configurations. It is sufficient in practice to concentrate on the coefficients of the cosine terms in the Fourier expansion, since the sine terms give similar results. We then try to reconstruct S_P from this information.

There are potentially two obstacles to this approach. First, there are as many independent Fourier components as there are lattice sites in the V_3 volume, and this is too many to calculate in practice. Secondly, it might be that the results are strongly dependent on the particular thermalized background which is used. Concerning the first obstacle, this will not be a problem if the derivatives with respect to $a_{\boldsymbol{k}}$ have a simple dependence on the lattice momentum

$$k_L = \sqrt{4\sum_{i=1}^{3}\sin^2(\frac{1}{2}k_i)} , \tag{11}$$

which can be deduced from a small sample of all possible components. As for the second obstacle,

5

this is not a problem if it turns out that the dependence of the final results on the particular choice of thermalized configuration is very weak.

A. Deriving the effective PLA

The first step in the extrapolation to small α is to run a standard lattice Monte Carlo, stop at some thermalized configuration, and calculate all the Polyakov line holonomies,

$$
\begin{aligned}
\mathscr{P}_{\boldsymbol{x}} &= U_0(\boldsymbol{x},1)U_0(\boldsymbol{x},2)...U_0(\boldsymbol{x},N_t) \\
&= d_4(n_1,n_2,n_3)\mathbb{1} + i\boldsymbol{d}(n_1,n_2,n_3)\cdot\boldsymbol{\sigma} ,
\end{aligned}
\tag{12}
$$

where $\boldsymbol{x} = (n_1,n_2,n_3)$, in that configuration. Define $W(\boldsymbol{x}) = d_4(\boldsymbol{x})$. We pick a particular wavevector $\boldsymbol{k}$ which is specified by three integers (m_1,m_2,m_3) with corresponding wavenumber components

$$
k_i = \frac{2\pi}{L}m_i ,
\tag{13}
$$

and set the coefficient of $\cos(\boldsymbol{k}\cdot\boldsymbol{x})$, in the sine-cosine expansion of $W(\boldsymbol{x})$, to zero. Denote the modified array, with the $\cos(\boldsymbol{k}\cdot\boldsymbol{x})$ term removed, as $W'(\boldsymbol{x})$.

Next, construct a set of $M = 20$ configurations with:

$$
\begin{aligned}
P_{\boldsymbol{x}}^{(n)} &= a_{\boldsymbol{k}}^{(n)}\cos(k_1 n_1 + k_2 n_2 + k_3 n_3) + (1-\alpha-\delta)W'(\boldsymbol{x}) \\
a_{\boldsymbol{k}}^{(n)} &= \alpha + \left(n - \frac{1}{2}(M+1)\right)\gamma/L^3 \quad, \quad n = 1,2,...,M ,
\end{aligned}
\tag{14}
$$

where $\gamma = L^3\Delta a$ is a constant chosen to be as small as possible, but still large enough to get some spread in the data. Typically $\gamma \approx 0.5$.

The factor $1-\alpha-\delta$ in (14) is introduced in order to keep $P_{\boldsymbol{x}}^{(n)}$, with rare exceptions, inside the range $[-1:1]$. Ideally one would like to leave all $\{a_{\boldsymbol{k}'},b_{\boldsymbol{k}'}\}$ in the thermalized configuration unaltered, apart from the mode with $\boldsymbol{k}' = \boldsymbol{k}$, i.e. $P_{\boldsymbol{x}}^{(n)} = a_{\boldsymbol{k}}\cos\boldsymbol{k}\cdot\boldsymbol{x} + W'(\boldsymbol{x})$. At finite α, however, this has the disadvantage that at many sites $|P_{\boldsymbol{x}}| > 1$. To see this, note that $W(\boldsymbol{x})$, from which $W'(\boldsymbol{x})$ is derived, may come close to the limits ± 1 at some sites, and at these sites the additional contribution $a_{\boldsymbol{k}}\cos(\boldsymbol{k}\cdot\boldsymbol{x})$ may put the sum outside the allowed range by as much as α. Moreover, by removing the $\cos(\boldsymbol{k}\cdot\boldsymbol{x})$ mode, $W'(\boldsymbol{x})$ may already lie outside the range $[-1:1]$ at some sites; this is especially true for $\boldsymbol{k} = 0$. We must also allow for the fact that half of the $\{a_{\boldsymbol{k}}^{(n)}\}$ are slightly greater than α. For this reason we reduce the amplitude of the added thermalized configuration by a factor of $1-\alpha-\delta$ (in our simulations we found $\delta = .04$ sufficient). In the exceptional cases where $P_{\boldsymbol{x}}^{(n)}$ still lies outside the allowed range, it is truncated to the nearest limit, i.e. ± 1.

We then construct the SU(2) variables, at each site, which have $2P_{\boldsymbol{x}}^{(n)}$ as the trace

$$
U_{\boldsymbol{x}}^{(n)} = P_{\boldsymbol{x}}^{(n)}\mathbb{1} + is^{(n)}\boldsymbol{d}(\boldsymbol{x})\cdot\boldsymbol{\sigma} ,
\tag{15}
$$

where, to insure unitarity,

$$
s^{(n)} = \sqrt{\frac{1 - (P_{\boldsymbol{x}}^{(n)})^2}{\boldsymbol{d}(\boldsymbol{x})\cdot\boldsymbol{d}(\boldsymbol{x})}} .
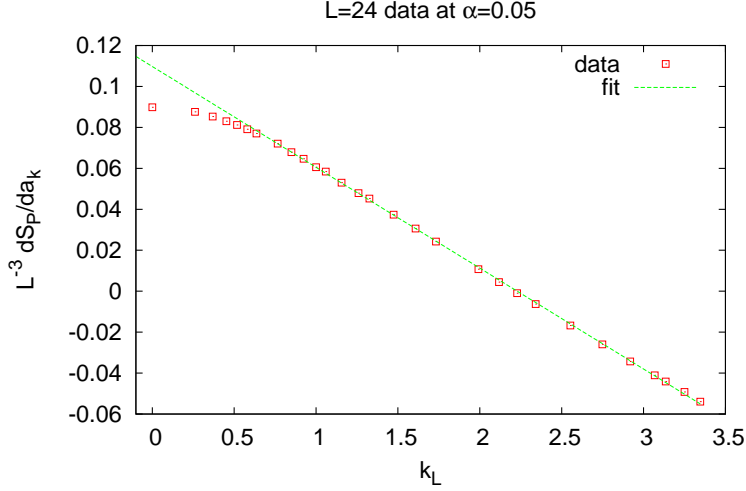\tag{16}
$$

6

FIG. 1. Derivatives of the PLA $L^{-3}\partial S_P/\partial a_{\boldsymbol{k}}$ evaluated at $a_{\boldsymbol{k}} = \alpha = 0.05$, vs. lattice momenta k_L. Also shown is a linear best fit to the data at $k_L > 0.7$.

The calculation of $(\partial S_P/\partial a_{\boldsymbol{k}})_\alpha$ proceeds as described above. For the choice of $U^{(n)}$ given above, it is easy to see that for a lattice of extension L in the spatial directions

$$\frac{1}{L^3}\left(\frac{\partial S_P[U_{\boldsymbol{x}}(a_{\boldsymbol{k}})]}{\partial a_{\boldsymbol{k}}}\right)_{a_{\boldsymbol{k}}=\alpha} \approx \frac{1}{\gamma(M-1)}\sum_{m=1}^{M-1}\log\left(\left\langle\exp\left[\Delta S^{(m+1)}[U]\right]\right\rangle_m\right) . \tag{17}$$

The results for the derivatives are found to depend only weakly on the particular choice of thermalized configuration, generated in an ordinary Monte Carlo run, which provides us with a set of Polyakov line holonomies (12) . The dependence is most pronounced at small k_L, with the variance on the order of 2%. In practice we have averaged our results for $dS_P/da_{\boldsymbol{k}}$ over eighty independent sets of Polyakov line holonomies, generated from the same number of thermalized lattice configurations.

In Fig. 1 we display our results for the $L^{-3}dS_P/da_{\boldsymbol{k}}$ vs. k_L at $\alpha = 0.05$, and lattice spatial extension $L = 24$. (Note that, apart from Figs. 5 and 7, all our figures show data derived at an $L = 24$ extension.) The underlying SU(2) lattice gauge theory is defined as a Wilson action on a periodic $24^3 \times 4$ volume, at the coupling $\beta = 2.2$. The calculations were made, in this case, at lattice momenta with components $k_i = 2\pi m_i/L$, with the following $(m_1 m_2 m_3)$ triplets:

$$\begin{aligned}\Big\{&(000),(100),(110),(111),(200),(210),(211),(300),(311),(320),\\&(400),(322),(421),(430),(333),(433),(443),(444),(554),(654),\\&(655),(665),(766),(777),(887),(988),(998),(10\,99),(10\,10\,10)\Big\} .\end{aligned} \tag{18}$$

On this plot the data point displayed at $k_L = 0$ is a factor of two smaller than the actual data value; this was done for reasons to be explained shortly.

The striking thing about this data is that, for lattice momenta $k_L > 0.7$, the data points clearly fall on a straight line. The second fact is that the data is linearly proportional to α at these small α values, as we see in Fig. 2. In this figure we divide $dS_P/da_{\boldsymbol{k}}$ by α, at $\alpha = 0.05, 0.10, 0.15, 0.20$, and find that the data points coincide. The linearity of the derivative w.r.t. $a_{\boldsymbol{k}}$ implies that the action
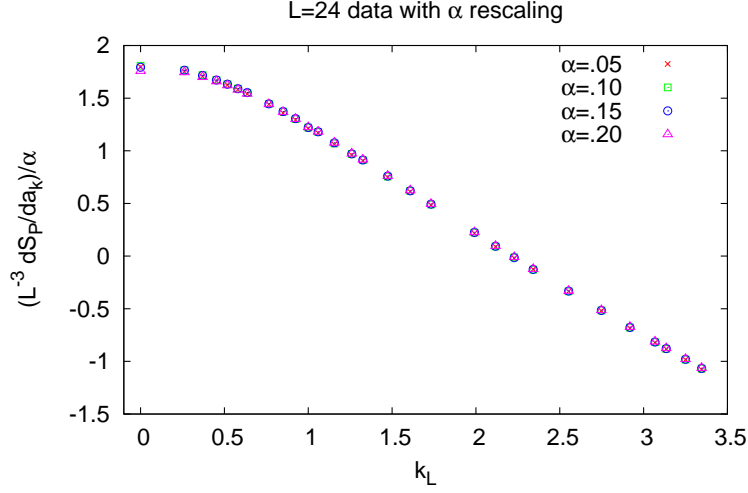
FIG. 2. Derivatives $L^{-3}(\partial S_P/\partial a_k)_\alpha$ divided by α, vs. lattice momenta k_L, for $\alpha = 0.05, 0.10, 0.15, 0.20$. It is clear that the derivatives of S_P depend linearly on α.

itself is quadratic in these variables, leading to a simple bilinear form

$$S_P = \frac{1}{2}c_1 \sum_x P_x^2 - 2c_2 \sum_{xy} P_x Q(x-y)P_y \,, \tag{19}$$

where

$$Q(x-y) = \frac{1}{L^3} \sum_k \widetilde{Q}(k_L)e^{ik \cdot (x-y)} \,. \tag{20}$$

This leads to derivatives

$$\frac{1}{L^3}\left(\frac{dS_P[U_x(a_k)]}{da_k}\right)_{a_k=\alpha} = \begin{cases} \alpha(\frac{1}{2}c_1 - 2c_2\widetilde{Q}(k_L)) \ \ k_L \neq 0 \\[2mm] 2\alpha(\frac{1}{2}c_1 - 2c_2\widetilde{Q}(0)) \ \ k_L = 0 \end{cases} \,. \tag{21}$$

The relative factor of two in the $k_L = 0$ and $k_L > 0$ cases is due to the fact that $\sum_x 1 = L^3$, while $\sum_x \cos^2(k \cdot x) = \frac{1}{2}L^3$. The $k_L > 0$ data should extrapolate, as $k_L \to 0$, to a value which is half the result at $k_L = 0$, which is why we have divided the derivative at $k_L = 0$ by a factor of 2, when displaying these values on Figs. 1 and 2. The constants c_1 and c_2 are obtained from a linear fit to the data at $k_L > 0.7$, as shown in Fig. 1.[1]

It is clear that for $k_L > 0.7$, the k-space kernel is $\widetilde{Q}(k_L) = k_L$. If this were true at all k_L, then we would have $Q = \sqrt{-\nabla_L^2}$ in position space, where $-\nabla_L^2$ is the negative lattice Laplacian

$$(-\nabla_L^2)_{xy} = \sum_{i=1}^3 (2\delta_{xy} - \delta_{x,y+\hat{i}} - \delta_{x+\hat{i},y}) \,. \tag{22}$$

---

[1] In practice we fit the data for each α, at $k_L > 0.7$, to the form $A(\alpha) - B(\alpha)k_L$. We then fit $A(\alpha)$, $B(\alpha)$ to straight lines, and the constants c_1, c_2 are extracted from the slopes, i.e. $dA/d\alpha = \frac{1}{2}c_1$, and $dB/d\alpha = 2c_2$. The choice of 0.7 as the lower limit is a potential source of systematic error, since the value for c_1 can vary up to 1% when the lower limit is increased (the variation of c_2 is smaller). We find, however, that the choice of 0.7 as the lower limit minimizes the reduced χ^2 value of the linear fit.
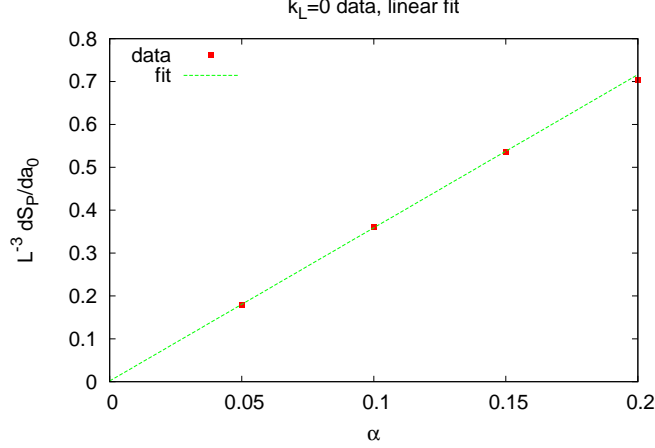
FIG. 3. The derivatives of S_P with respect to the amplitude of the zero mode, evaluated at several values of α. The slope of this data is used to determine r_{max} of the bilinear kernel $Q(\mathbf{x} - \mathbf{y})$, as explained in the text.

However, a kernel $Q(\mathbf{x} - \mathbf{y})$ of this kind is infinite range, which would violate one of the assumptions of the Svetitisky-Yaffe analysis (cf. [12]). In any case, comparing Fig. 2 with eq. (21), it is clear that $\widetilde{Q}(k_L)$ must deviate from linearity at small momentum. We therefore make an ansatz for the kernel which imposes the finite range restriction on Q in a simple way:

$$Q(\mathbf{x} - \mathbf{y}) = \begin{cases} \left(\sqrt{-\nabla_L^2}\right)_{xy} & |\mathbf{x} - \mathbf{y}| \leq r_{max} \\ 0 & |\mathbf{x} - \mathbf{y}| > r_{max} \end{cases} . \tag{23}$$

Given r_{max}, $\widetilde{Q}(k_L)$ is obtained by a Fourier transform of $Q(\mathbf{x} - \mathbf{y})$, and this result can be compared to the data via (21). Actually, two Fourier transforms are required. First, we determine $\left(\sqrt{-\nabla_L^2}\right)_{xy}$ from

$$\left(\sqrt{-\nabla_L^2}\right)_{xy} = \frac{1}{L^3} \sum_{\mathbf{k}} k_L e^{i\mathbf{k} \cdot (\mathbf{x} - \mathbf{y})} . \tag{24}$$

and eq. (23) defines $Q(\mathbf{x} - \mathbf{y})$, given r_{max} (see Table II). Then $\widetilde{Q}(k_L)$ is derived from $Q(\mathbf{x})$ by inverting the transform (20).

To determine r_{max}, we do a linear fit of the $k_L = 0$ data

$$\frac{1}{L^3} \left(\frac{dS_P}{da_0}\right)_{a_0 = \alpha} \text{ vs. } \alpha , \tag{25}$$

as shown in Fig. 3. Let the slope of the line be D. Then, from (21),

$$c_1 - 4c_2 \widetilde{Q}(0)) = D , \tag{26}$$

The r_{max} cutoff fixes $Q(\mathbf{x} - \mathbf{y})$ via (23), and then $\widetilde{Q}(k_L)$ at all $\mathbf{k}$ is obtained by inverting the transform (20). We choose r_{max} to satisfy the condition (26) as closely as possible.
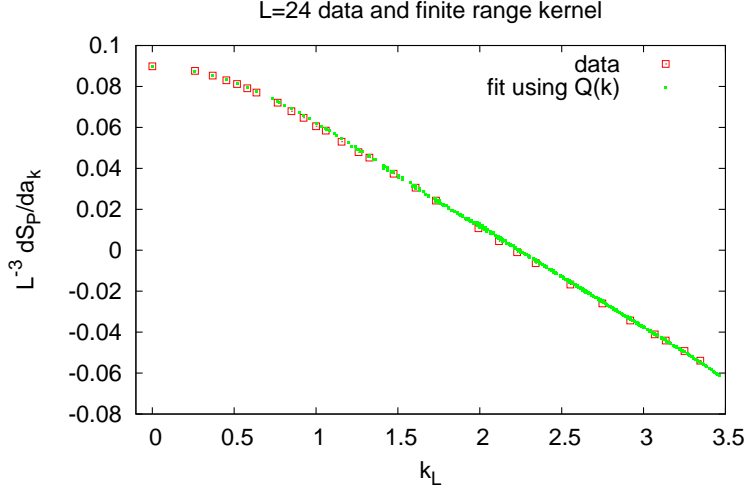
FIG. 4. A test of eq. (21) at $\alpha = 0.05$. The derivative data of Fig. 1 is plotted against the conjectured fitting function $\alpha(\frac{1}{2}c_1 - 2c_2\widetilde{Q}(k_L))$ with $r_{max} = 3$.

In Fig. 4 we plot the data shown in Fig. 1 together with the values computed for

$$\alpha(\frac{1}{2}c_1 - 2c_2\widetilde{Q}(k_L)) \tag{27}$$

(cf. eq. (21)) at $\alpha = 0.05$. Agreement seems to be quite good in the entire range of k_L.

We have repeated this analysis at smaller volumes of spatial extension $L = 12, 16, 20$. The results for c_1, c_2, r_{max} are shown in Table I. In Table II we record non-zero components of $Q(\mathbf{x}) = (-\nabla_L^2)_{\mathbf{x}0}$ up to $|\mathbf{x}| < 3.2$ and lattice volume 24^3. For $r_{max} = 3$, the last entry in the table should be replaced by $Q(3,1,0) = 0$. The rest of the non-zero elements of Q are obtained from the table via permutation symmetry, $x_i \leftrightarrow x_j$, and reflection symmetry $x_i \to -x_i$, among the coordinate components.

L	c_1	c_2	r_{max}
12	4.364(6)	0.491(1)	3.2
16	4.417(4)	0.498(1)	3.0
20	4.416(7)	0.493(1)	3.0
24	4.414(8)	0.493(1)	3.0

TABLE I. Constants defining the effective Polyakov line action for pure YM theory, $L^3 \times 4$ lattice, $\beta = 2.2$.

B. Comparing the PLA to the underlying lattice gauge theory

We now have a concrete proposal for the effective Polyakov line actions at various spatial volumes L^3 ranging from 12^3 to 24^3, and which correspond to an underlying lattice SU(2) gauge theory at $\beta = 2.2$ on an $L^3 \times 4$ lattice volume. The actions are specified by eqs. (19), (23), and the constants in Table I. Above the lattice volume 12^3, these actions are about the same.

10

x_1	x_2	x_3	$Q(\boldsymbol{x})$
0	0	0	2.38760
1	0	0	-0.22001
1	1	0	-0.02357
1	1	1	-0.00774
2	0	0	-0.01279
2	1	0	-0.00455
2	1	1	-0.00246
2	2	0	-0.00160
2	2	1	-0.00111
3	0	0	-0.00200
3	1	0	-0.00121

TABLE II. Non-zero elements of the bilinear kernel $Q(\boldsymbol{x})$ at $r_{max} = 3.2$ and $L = 24$.
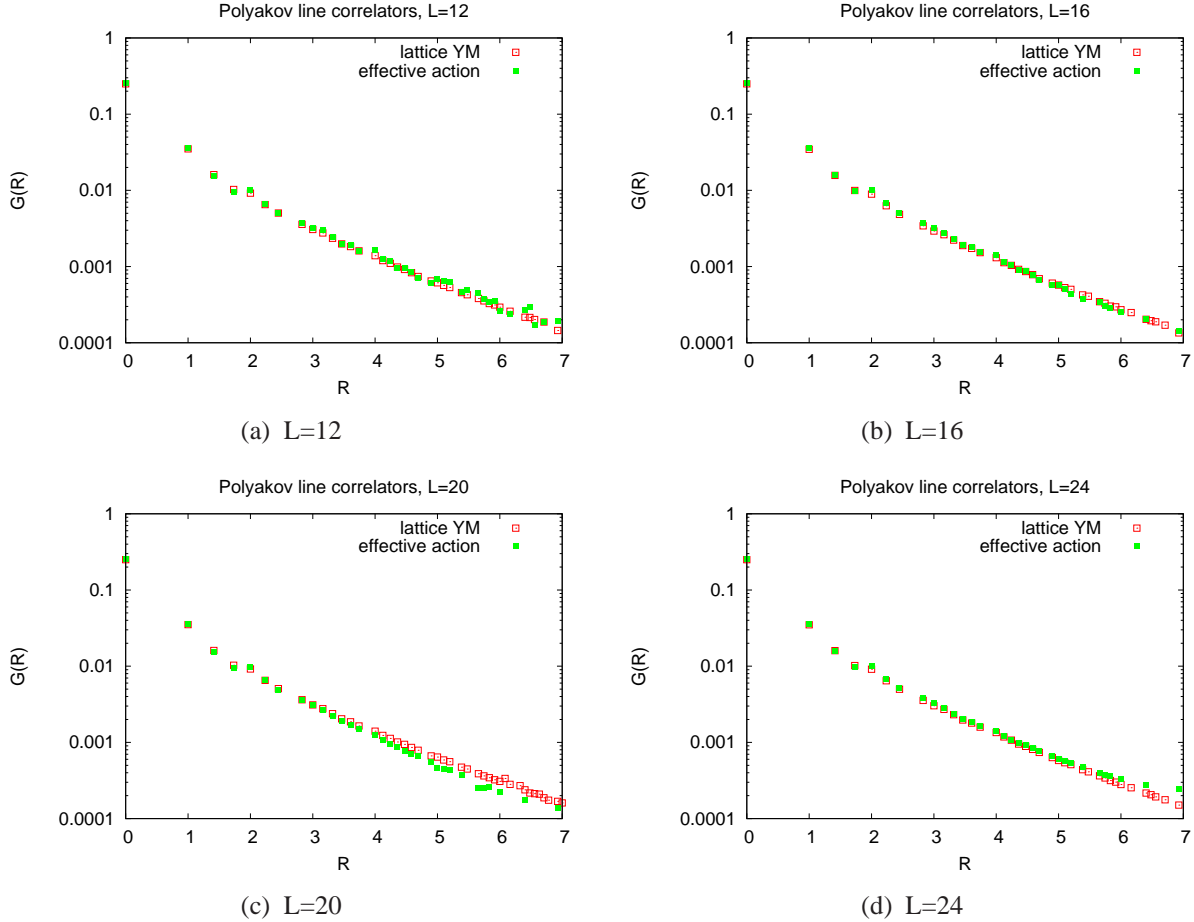

(a) L=12

(b) L=16

(c) L=20

(d) L=24

FIG. 5. A comparison of the Polyakov line correlation functions $G(|\boldsymbol{x} - \boldsymbol{y}|) = \langle P_{\boldsymbol{x}} P_{\boldsymbol{y}} \rangle$ as computed via lattice Monte Carlo simulation of the underlying gauge theory on a $L^3 \times 4$ lattice at coupling $\beta = 2.2$, and via Monte Carlo simulation of the corresponding effective action S_P of eq. (19). Lattices are of spatial extension $L = 12, 16, 20, 24$ lattice spacings. Note that off-axis displacements are included.
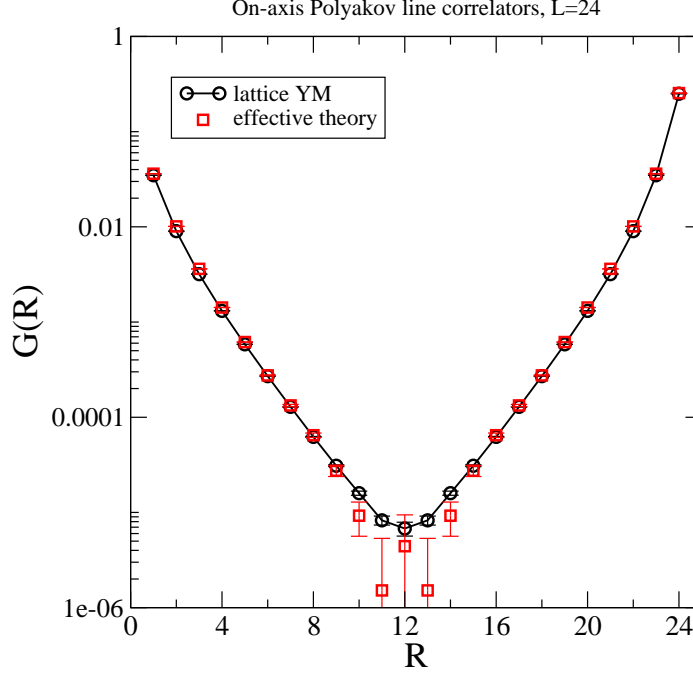
FIG. 6. A high-statistics comparison of the Polyakov line correlation function $G(|\boldsymbol{x}-\boldsymbol{y}|) = \langle P_{\boldsymbol{x}} P_{\boldsymbol{y}} \rangle$ computed for the lattice gauge and effective theories, for displacements $\boldsymbol{x}-\boldsymbol{y}$ parallel to the x, y or z-axes, and spatial volume 24^3.

The crucial question, of course, is whether these proposed Polyakov line actions are correct; they are certainly different from the action suggested in ref. [6], which was derived for gauge configurations in a rather unrepresentative region of configuration space. There is one obvious and essential test: Do the derived Polyakov line actions reproduce the Polyakov line correlator calculated in the corresponding lattice gauge theory? Thus we compute, via numerical simulation of the Polyakov line action at $L = 12, 16, 20, 24$,

$$G(|\boldsymbol{x}-\boldsymbol{y}|) = \langle P_{\boldsymbol{x}} P_{\boldsymbol{y}} \rangle \,, \tag{28}$$

and compare the result to the same observable obtained from standard lattice Monte Carlo at $\beta = 2.2$ on an $L^3 \times 4$ volume. The result for these four cases is shown in Fig. 5. Note that off-axis displacements are included, with xyz-components of the displacement $\boldsymbol{x}-\boldsymbol{y}$ in the range $[-4, 4]$.

The data in Fig. 5 is limited to displacements of magnitude $R < 7$ lattice spacings, and it is interesting to consider larger displacements for larger lattices. This calls for higher statistics. In Fig. 6 we compare the results for $G(\boldsymbol{x}-\boldsymbol{y})$ obtained on a 24^3 lattice for the effective theory, and on a $24^3 \times 4$ lattice for the SU(2) gauge theory, again at $\beta = 2.2$. In this figure we show the results for displacements $\boldsymbol{x}-\boldsymbol{y}$ parallel to any one of the coordinate axes. The Lüscher-Weisz noise reduction method [13] was used in obtaining the Polyakov line correlator in the lattice gauge theory, while for the effective Polyakov line action the correlator was obtained from 38,400 configurations (about two orders of magnitude more than was used in Fig. 5).

The agreement of the correlators in the PLA and the underlying lattice gauge theory seen in Fig. 6 is extraordinary, and it persists down to magnitudes of order 10^{-5}.[2] While this is not a

---

[2] The Polyakov line correlator derived from the Inverse Monte Carlo method in ref. [8] was displayed on a linear, rather than logarithmic, scale, and hence the precision of agreement with lattice gauge theory, in that approach, is difficult to judge.

proof that S_P is the correct effective action, it is difficult to believe that agreement of Polyakov line correlators to this level of precision is coincidental.

IV. POLYAKOV LINE ACTION FOR AN SU(2) GAUGE-HIGGS SYSTEM

We now add a scalar matter field in the fundamental representation of the gauge group, thereby breaking explicitly Z_2 center symmetry. The simplest case is a fixed-modulus Higgs field, and for SU(2) gauge theory the action can be written in the following way:

$$S = \beta \sum_{plaq} \frac{1}{2} \text{Tr}[UUU^\dagger U^\dagger] + \kappa \sum_{x,\mu} \frac{1}{2} \text{Tr}[\phi^\dagger(x)U_\mu(x)\phi(x+\widehat{\mu})] \ , \qquad (29)$$

where $\phi(x)$ is SU(2) group-valued. The work of Fradkin and Shenker [14], itself based on a theorem by Osterwalder and Seiler [15], demonstrated that the Higgs region and the "confinement-like" regions of the $\beta - \kappa$ phase diagram are continuously connected. Subsequent Monte Carlo studies found that there is only a single phase at zero temperature (there might have been a separate Coulomb phase), although there is a line of first-order transitions between the confinement-like and Higgs regions, which eventually turns into a line of sharp crossover around $\beta = 2.775, \kappa = 0.705$, cf. [16] and references therein. At $\beta = 2.2$ the crossover occurs at $\kappa \approx 0.84$, as seen in the plaquette energy data shown in Fig. 7. There is also a steep rise in the Polyakov line expectation value as κ increases past this point.
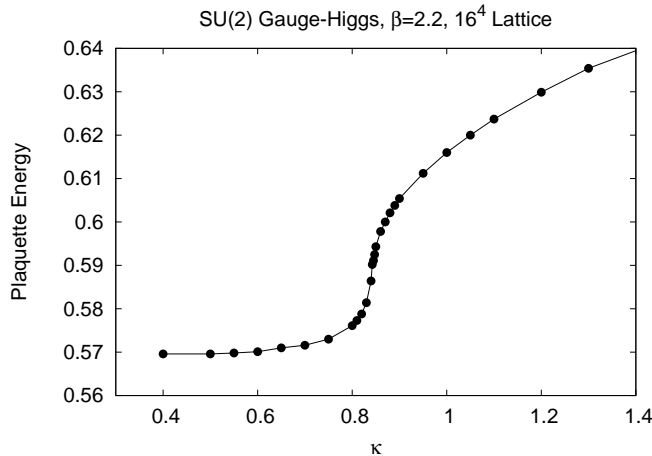

FIG. 7. Plaquette energy vs. gauge-Higgs coupling κ at fixed $\beta = 2.2$, for the SU(2) gauge-Higgs theory with fixed Higgs modulus on a 16^4 lattice volume, showing a sharp crossover at $\kappa \approx 0.84$.

We will work at $\beta = 2.2$ on a $24^3 \times 4$ lattice volume, but this time at Higgs coupling $\gamma = 0.75$, which places us in the "confinement-like" phase a little below the crossover point. For these parameters, the Polyakov line has a VEV of $\langle P_x \rangle = 0.0515$. Once again, we generate sets of thermalized Polyakov line holonomies, and compute $L^{-3} dS_P / da_k$ as explained in the previous section.

The derivatives $\partial S_P / \partial a_k$ at $a_k = \alpha$ are computed as before, and at each $k_L > 0$ the results are simply proportional to α. The constants c_1, c_2 are again extracted by a linear fit to the $k_L > 0.7$ data. However, the data at $k_L = 0$ is not strictly proportional to α; there is also an α-independent constant contribution to the data. This fact can be seen in Fig. 8. The straight line is a best fit to
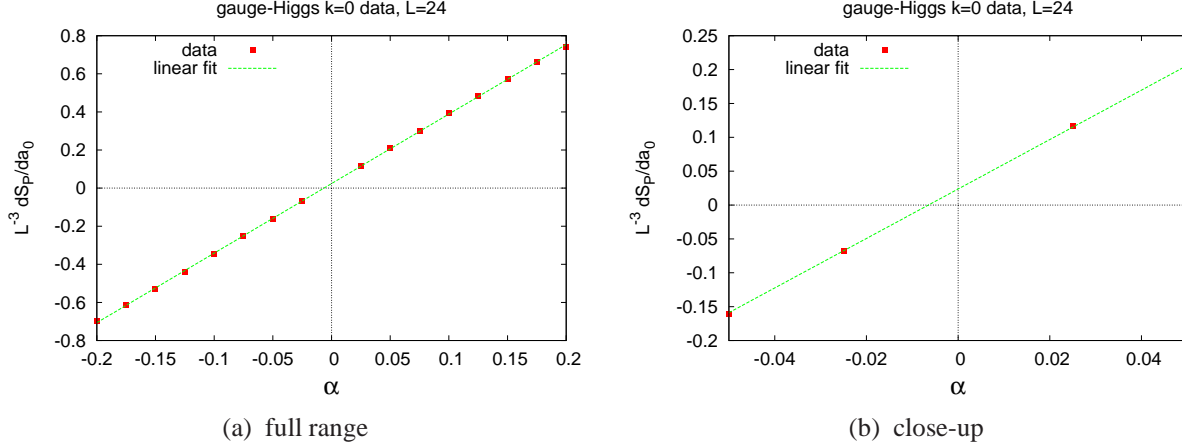
13

(a) full range   (b) close-up

FIG. 8. The derivatives of S_P with respect to the amplitude of the zero mode in the gauge-Higgs theory, evaluated at positive and negative values of $a_0 = \alpha$. (a) shows the full range of the data; (b) is a closeup near $\alpha = 0$. The y-intercept of this data is non-zero, and determines the coefficient c_0 of the linear, Z_2-symmetry breaking term in the effective PLA (30).

$L^{-3} \partial S_P / \partial a_0$ evaluated at $a_0 = \alpha$ for α in the range $[-0.2, 0.2]$. The y-intercept of this line does not pass through zero, but rather through $y = 0.0236(14)$. This implies that S_P must contain a term which is linear in $P_{\boldsymbol{x}}$, i.e.

$$S_P = c_0 \sum_{\boldsymbol{x}} P_{\boldsymbol{x}} + \frac{1}{2} c_1 \sum_{\boldsymbol{x}} P_{\boldsymbol{x}}^2 - 2 c_2 \sum_{\boldsymbol{xy}} P_{\boldsymbol{x}} Q(\boldsymbol{x} - \boldsymbol{y}) P_{\boldsymbol{y}} , \tag{30}$$

and it is clear from inspection that c_0 must equal to the y-intercept in Fig. 8. It is also clear that only the $k_L = 0$ mode contributes to the linear term, and is therefore invisible in the derivatives of S_P at $k_L > 0$. We define $Q(\boldsymbol{x} - \boldsymbol{y})$ again by (23), with r_{max} determined as in the pure-gauge theory. The final set of parameters for the effective Polyakov line action is given in Table III, and we plot the $k_L > 0$ data, together with the quantity

$$\alpha(\frac{1}{2} c_1 - 2 c_2 \widetilde{Q}(k_L)) \quad \text{vs.} \quad k_L \tag{31}$$

in Fig. 9.

L	c_0	c_1	c_2	r_{max}
24	.0236(14)	4.447(9)	0.501(1)	3.2

TABLE III. Constants defining the effective Polyakov line action for gauge-Higgs theory, $24^3 \times 4$ lattice, $\beta = 2.2$, $\kappa = 0.75$.

As in the pure gauge theory, the crucial test is to see whether the Polyakov line correlator (28) found from numerical simulation of the gauge-Higgs theory (29) agrees with the same observable computed in the derived Polyakov line action (30). The results are shown in Fig. 10. In this case the agreement between the lattice gauge Higgs correlator (black diamonds) and the correlator of the effective action (blue triangles), while fairly close, is not perfect. However, the result for the
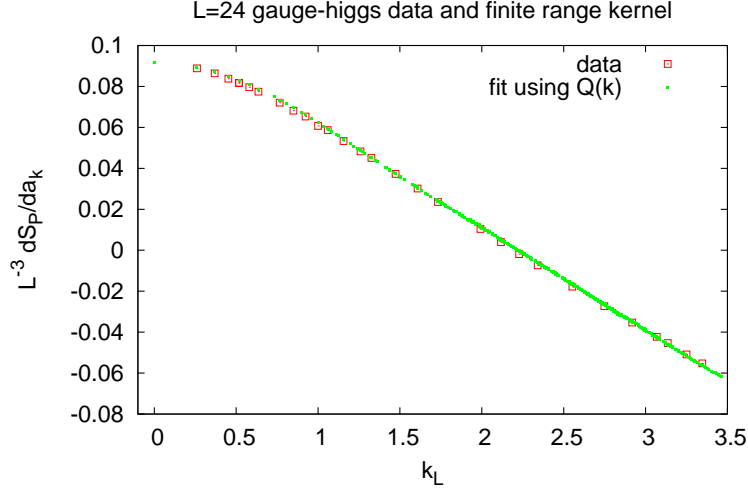
14

FIG. 9. Same as Fig. 4 for the gauge-Higgs theory. We plot the data for the derivative $L^{-3}\partial S_P/\partial a_{\boldsymbol{k}}$ vs. k_L against the conjectured fitting function $\alpha(\frac{1}{2}c_1 - 2c_2\widetilde{Q}(k_L))$ with $r_{max} = 3.2$.
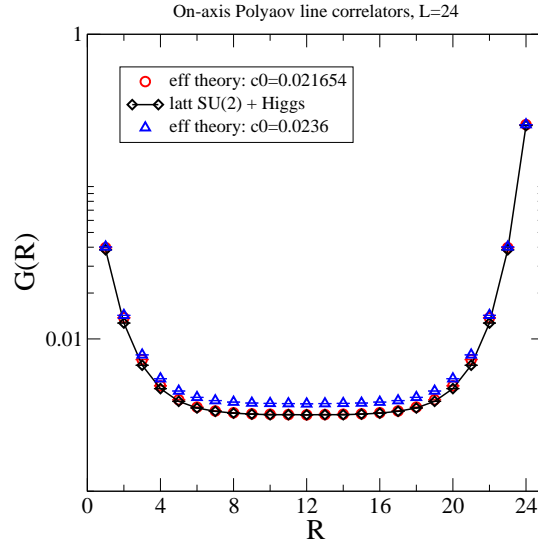

FIG. 10. A comparison of the Polyakov line correlation functions $G(|\boldsymbol{x} - \boldsymbol{y}|) = \langle P_{\boldsymbol{x}}P_{\boldsymbol{y}}\rangle$ as computed via lattice Monte Carlo simulation of the underlying gauge-Higgs theory (black diamonds) on a $24^3 \times 4$ lattice, at couplings $\beta = 2.2$, $\kappa = 0.75$, and via Monte Carlo simulation of the corresponding effective action S_P of eq. 30 (blue triangles, $c_0 = 0.0236$). Also shown is a simulation of the effective action with a slightly different value of $c_0 = .02165$ (red circles).

effective action depends very sensitively on the value of c_0, and of course there is an errorbar associated with this quantity. In our best fits, $c_0 = 0.0236(14)$. With a little trial and error, one can find a value of c_0 for the effective effective action such that the corresponding correlator (red circles) agrees almost exactly with the gauge-Higgs value. This happens at a value $c_0 = 0.02165$ which is not far outside our errorbars, about 1.4 σ away from $c_0 = 0.0236$.

15

V. S_P AT FINITE CHEMICAL POTENTIAL

As mentioned in the Introduction, one of our motivations in this work is to apply our methods to the well-known sign problem, which arises upon introducing a finite chemical potential to a system of matter fields coupled to gauge fields. There is no sign problem for the SU(2) gauge group, but the relative weights method should apply to other gauge groups as well, and to the SU(3) group in particular. However, since the method depends on ordinary Monte Carlo simulations, it is only applicable at chemical potential $\mu = 0$. Supposing, then, that we can compute the effective PLA for an SU(3) system at $\mu = 0$, how does this help us to find the effective theory at non-zero μ?

Recall that for small gauge coupling β and massive quark fields, the effective action $S_P^{\mu=0}$ at zero chemical potential, defined in temporal gauge by [3]

$$\exp\left[S_P^{\mu=0}[U_{\boldsymbol{x}}, U_{\boldsymbol{x}}^\dagger]\right] = \int DU_k D\overline{\psi} D\psi \, \exp\left[S_L[U_{\boldsymbol{x}}, U_{\boldsymbol{x}}^\dagger, U_i(x), \psi, \overline{\psi}]\right] . \tag{32}$$

can be computed from a combined strong-coupling/hopping parameter expansion of the functional integral on the right hand side. Let us consider any diagram D in an SU(N) gauge theory which contributes to this expansion. In general, after integrating out all spacelike link variables and fermion fields, the diagram (which may consist of some number of disconnected sub-diagrams) will contribute terms of the form

$$c_D N^{-p_D} \left(\frac{\beta}{2N^2}\right)^{p_D'} h^{p_D''} P_D[U_{\boldsymbol{x}}, U_{\boldsymbol{x}}^\dagger] \tag{33}$$

where h is the hopping parameter, c_D is a (β, h)-independent constant, p_D, p_D', p_D'' are integer powers, and $P_D[U_{\boldsymbol{x}}, U_{\boldsymbol{x}}^\dagger]$ is a product of traces of Polyakov line holonomies at various positions and of various winding numbers, i.e.

$$P_D[U_{\boldsymbol{x}}, U_{\boldsymbol{x}}^\dagger] = \text{Tr} U_{\boldsymbol{x}_1}^{w_1} \text{Tr} U_{\boldsymbol{x}_2}^{w_2} ... \text{Tr} U_{\boldsymbol{x}_n}^{w_n} \text{Tr} U_{\boldsymbol{y}_1}^{\dagger w_1'} \text{Tr} U_{\boldsymbol{y}_2}^{\dagger w_2'} ... \text{Tr} U_{\boldsymbol{y}_m}^{\dagger w_m'} \tag{34}$$

where the w_i, w_i' are winding numbers for Polyakov lines of opposite orientation.[4] Then

$$\exp\left[S_P^{\mu=0}[U_{\boldsymbol{x}}, U_{\boldsymbol{x}}^\dagger]\right] = \sum_D c_D N^{-p_D} \left(\frac{\beta}{2N^2}\right)^{p_D'} h^{p_D''} P_D[U_{\boldsymbol{x}}, U_{\boldsymbol{x}}^\dagger] \tag{35}$$

By standard arguments, the series can be resummed into an exponential whose exponent contains only connected diagrams.

Note that since $U_{\boldsymbol{x}}, U_{\boldsymbol{x}}^\dagger$ are unintegrated, it is irrelevant to the strong-coupling/hopping parameter expansion whether these matrices are unitary, or even whether, despite the notation, they are hermitian conjugates of one another, providing only that $U_{\boldsymbol{x}} U_{\boldsymbol{x}}^\dagger = \mathbb{1}$ at each $\boldsymbol{x}$.

Now in QCD, a chemical potential is introduced by making the replacement

$$U_{\boldsymbol{x}} \to e^{N_t \mu} U_{\boldsymbol{x}} \quad , \quad U_{\boldsymbol{x}}^\dagger \to e^{-N_t \mu} U_{\boldsymbol{x}}^\dagger \tag{36}$$

in the Dirac operator. But in fact, we can also formally make this replacement in the pure gauge

---

[3] The notation means that $U_0(\boldsymbol{x}, 0)$ is replaced by $U_{\boldsymbol{x}}$, and $U_0^\dagger(\boldsymbol{x}, 0)$ is replaced by $U_{\boldsymbol{x}}^\dagger$, in the lattice action S_L.

[4] Because of a residual gauge invariance $U_0(\boldsymbol{x}, 0) \to g_{\boldsymbol{x}} U_0(\boldsymbol{x}, 0) g_{\boldsymbol{x}}^\dagger$ in temporal gauge on a periodic lattice, there are no terms in P_D involving traces of products of holonomies at different sites, e.g. $\text{Tr} U_{\boldsymbol{x}}^w U_{\boldsymbol{y}}^{\dagger w'}$ with $\boldsymbol{x} \neq \boldsymbol{y}$.

part of the action as well, since this part is invariant under the replacement. This means that

$$S_L^\mu[U_x, U_x^\dagger, U_i(x), \psi, \overline{\psi}] = S_L[e^{N_t \mu} U_x, e^{-N_t \mu} U_x^\dagger, U_i(x), \psi, \overline{\psi}] \tag{37}$$

and therefore

$$\exp\left[S_P^\mu[U_x, U_x^\dagger]\right] = \int DU_k D\overline{\psi} D\psi \, \exp\left[S_L^\mu[U_x, U_x^\dagger, U_i(x), \psi, \overline{\psi}]\right]$$
$$= \int DU_k D\overline{\psi} D\psi \, \exp\left[S_L[e^{N_t \mu} U_x, e^{-N_t \mu} U_x^\dagger, U_i(x), \psi, \overline{\psi}]\right]. \tag{38}$$

Once again, we may compute the second line of (38) by a strong-coupling/hopping parameter expansion. As already noted, the fact that $e^{N_t \mu} U_x, e^{-N_t \mu} U_x^\dagger$ are non-unitary, and are not the hermitian conjugates of one another, is irrelevant to the expansion. We have exactly the same set of diagrams as in the $\mu = 0$ expansion, and for each contribution the constants c_D, p_D, p_D', p_D'' are unchanged. The *only* change is that the Polyakov line holonomies in P_D are modified by a factor of $e^{N_t \mu}$ multiplying U_x, and a factor of $e^{-N_t \mu}$ multiplying $U_x^\dagger$, i.e.

$$\exp\left[S_P^\mu[U_x, U_x^\dagger]\right] = \sum_D c_D N^{-p_D} \left(\frac{\beta}{2N^2}\right)^{p_D'} h^{p_D''} P_D[e^{N_t \mu} U_x, e^{-N_t \mu} U_x^\dagger] \tag{39}$$

Comparing (35) and (39), it is clear that there must be a simple and powerful identity, which is *exact* within the radius of convergence of the strong-coupling/hopping parameter expansion, relating S_P^μ to $S_P^{\mu=0}$, namely

$$S_P^\mu[U_x, U_x^\dagger] = S_P^{\mu=0}[e^{N_t \mu} U_x, e^{-N_t \mu} U_x^\dagger] \tag{40}$$

It is not unreasonable to assume that this relationship is valid in general, for arbitrary β, h. If so, and if we are able to compute $S_P^{\mu=0}[U_x, U_x^\dagger]$ by some method (such as relative weights), then we obtain the effective Polyakov line action at non-zero chemical potential by the trivial replacement (36) in the effective Polyakov line action at zero chemical potential.[5] Remarkably, this means that the effective Polyakov line action at $\mu \neq 0$ can in principle be obtained from the effective Polyakov action at $\mu = 0$, without actually simulating the underlying lattice gauge theory at non-zero μ.

VI. CONCLUSIONS

Motivated in part by the sign problem, we have applied the relative weights method to determine the effective Polyakov line action S_P for both pure and gauge-Higgs lattice SU(2) gauge theory. This effective action turns out to be a remarkably simple expression, which is bilinear in the Polyakov line variables $P_x = \frac{1}{2} \text{Tr}[U_x]$:

$$S_P = c_0 \sum_x P_x + \frac{1}{2} c_1 \sum_x P_x^2 - 2c_2 \sum_{xy} P_x Q(x-y) P_y$$
$$Q(x-y) = \begin{cases} \left(\sqrt{-\nabla_L^2}\right)_{xy} & |x-y| \leq r_{max} \\ 0 & |x-y| > r_{max} \end{cases}, \tag{41}$$

---

[5] For a discussion of a possible pitfall in this approach, and its resolution, cf. [4].

with $c_0 = 0$ in the pure-gauge theory, and non-zero in the gauge-Higgs theory. Our results so far have been obtained at lattice coupling $\beta = 2.2$, and $N_t = 4$ lattice spacings in the time direction. The effective action has been checked by computing Polyakov line correlators in both the effective theory and the underlying gauge theory, and we have found that these correlators agree quite well with each other. This is especially true in the pure gauge theory, where agreement persists down to correlator values of order 10^{-5}. These results, together with previous checks in the case of strong coupling [6], inspire some confidence that the method works. The next immediate step will be to understand how the couplings of the effective theory evolve as a function of coupling β and temperature $1/N_t$.

In the longer term our interest is the sign problem, and to address that problem it will be necessary to derive the effective Polyakov line action corresponding to lattice SU(3) gauge fields coupled to matter at zero chemical potential. As explained in the preceding section, we expect to extract the Polyakov line action at finite μ from the appropriate Polyakov line action at $\mu = 0$ by the simple substitution (36). The strategy is then to apply one or more of the methods [1–4], which were developed for solving Polyakov line actions with a chemical potential, to our derived effective action. If the sign problem is tractable in the effective Polyakov line theory, as suggested by the earlier work cited above, then it may be possible to extract useful results regarding the QCD phase diagram.

ACKNOWLEDGMENTS

Appendix: Dynamical Fermions

In this appendix we will just sketch how the relative weights algorithm can be applied in the case where there are two mass-degenerate dynamical fermions coupled to the gauge field.

Taking D as the Dirac operator, and $M \equiv D^\dagger D$, the integration measure is

$$e^{S_L} = \det M \; e^{S_W} , \tag{A.1}$$

where S_W is the Wilson (or other improved pure-gauge) action. Defining

$$M^{(m)} = M\left[U_0(\boldsymbol{x},0) = U_{\boldsymbol{x}}^{(m)}, U_k(x,t)\right] , \tag{A.2}$$

we have

$$\exp[\Delta S_P^{(m+1)}] = \frac{Z_{m+1}}{Z_m}$$
$$= \left\langle \frac{\det M^{(m+1)}}{\det M^{(m)}} \exp[\Delta S_W^{m+1}] \right\rangle_m , \tag{A.3}$$

where $\langle...\rangle_m$ signifies, as before, the expectation value in a probability measure $\exp[S_L^{(m)}]/Z_m$. The VEV can be evaluated via hybrid Monte Carlo, but in this case there is the question of how

to evaluate the ratio of determinants in (A.3). In the most straightforward approach, defining $\delta M^{(m+1)} = M^{(m+1)} - M^{(m)}$ and writing

$$\det M^{(m+1)} = \det\left\{ M^{(m)}(\mathbb{1} + [M^{(m)}]^{-1}\delta M^{(m+1)}) \right\}, \tag{A.4}$$

it is not hard to see that

$$\begin{aligned}
\frac{\det M^{(m+1)}}{\det M^{(m)}} &= \exp\left[\mathrm{Tr}\log\left\{ \mathbb{1} + [M^{(m)}]^{-1}\delta M^{(m+1)} \right\} \right] \\
&\approx \exp\left[\mathrm{Tr}\left\{ [M^{(m)}]^{-1}\delta M^{(m+1)} \right\} \right].
\end{aligned} \tag{A.5}$$

Therefore

$$\exp[\Delta S_P^{(m+1)}] = \left\langle \exp\left[\mathrm{Tr}\left\{ [M^{(m)}]^{-1}\delta M^{(m+1)} \right\} \right] e^{\Delta S_W^{(m+1)}} \right\rangle_m. \tag{A.6}$$

It is best not to evaluate the trace $\mathrm{Tr}\{[M^{(m)}]^{-1}\delta M^{(m+1)}\}$ directly, because of the computational expense, but rather indirectly, by the method of "noisy pseudofermions" (c.f. section 8.4 in ref. [17]).

A way of completely avoiding M^{-1} in the observable is to introduce another set of pseudofermions φ, distinct from the pseudofermions used by hybrid Monte Carlo, so that we may write

$$\frac{\det M^{(m+1)}}{\det M^{(m)}} = \frac{\int D\varphi \exp[-\varphi^\dagger M^{(m)}\varphi]}{\int D\varphi \exp[-\varphi^\dagger M^{(m+1)}\varphi]}. \tag{A.7}$$

Defining

$$\Delta A^{(m+1)} = \varphi^\dagger M^{(m+1)}\varphi - \varphi^\dagger M^{(m)}\varphi, \tag{A.8}$$

we have

$$\frac{\det M^{(m+1)}}{\det M^{(m)}} = \left\langle\!\!\left\langle \exp[\Delta A^{(m+1)}] \right\rangle\!\!\right\rangle_{m+1}, \tag{A.9}$$

where $\langle\!\langle ...\rangle\!\rangle_{m+1}$ refers to the expectation value in the measure proportional to

$$\exp[-\varphi^\dagger M^{(m+1)}\varphi]. \tag{A.10}$$

The final result for the relative weight is

$$\exp[\Delta S_P^{(m+1)}] = \left\langle \left\langle\!\!\left\langle \exp[\Delta A^{(m+1)}] \right\rangle\!\!\right\rangle_{m+1} \exp[\Delta S_W^{(m+1)}] \right\rangle_m. \tag{A.11}$$

Again, the expectation value $\langle ...\rangle_m$ would be computed via the usual hybrid Monte Carlo algorithm. Eq. (A.11) is to be used, as before, to compute path derivatives, hopefully leading to an expression for the effective PLA at $\mu = 0$. The PLA with a finite chemical potential would then be obtained from the substitution (36).

Apart from computation cost, we believe that the addition of dynamical fermions does not pose any problems of principle to the derivation of the effective Polyakov line action via the relative

19

weights approach.

[1] C. Gattringer, Nucl.Phys. **B850**, 242 (2011), arXiv:1104.2503.
    Y. D. Mercado and C. Gattringer, Nucl.Phys. **B862**, 737 (2012), arXiv:1204.6074.

[2] M. Fromm, J. Langelage, S. Lottini, and O. Philipsen, JHEP **1201**, 042 (2012), arXiv:1111.4953.

[3] G. Aarts and F. A. James, JHEP **1201**, 118 (2012), arXiv:1112.4655.

[4] J. Greensite and K. Splittorff, (2012), arXiv:1206.1159.

[5] P. de Forcrand, PoS **LAT2009**, 010 (2009), arXiv:1005.0539.

[6] J. Greensite, Phys.Rev. **D86**, 114507 (2012), arXiv:1209.5697.

[7] J. Greensite, H. Matevosyan, Š. Olejník, M. Quandt, H. Reinhardt, and A.P. Szczepaniak, Phys.Rev. **D83**, 114509 (2011), arXiv:1102.3941.
    J. Greensite and J. Iwasaki, Phys. Lett. **B223**, 207 (1989).

[8] L. Dittmann, T. Heinzl, and A. Wipf, JHEP **0406**, 005 (2004), arXiv:hep-lat/0306032.
    T. Heinzl, T. Kaestner, and A. Wipf, Phys.Rev. **D72**, 065005 (2005), arXiv:hep-lat/0502013.

[9] A. Velytsky, Phys.Rev. **D78**, 034505 (2008), arXiv:0805.4450.
    C. Wozar, T. Kastner, B. H. Wellegehausen, A. Wipf, and T. Heinzl, PoS **LATTICE2008**, 257 (2008), arXiv:0808.4046.

[10] A. Dumitru, Y. Guo, Y. Hidaka, C. P. K. Altes, and R. D. Pisarski, Phys.Rev. **D86**, 105017 (2012), arXiv:1205.0137.

[11] K. Langfeld and G. Shin, Nucl.Phys. **B572**, 266 (2000), arXiv:hep-lat/9907006.

[12] B. Svetitsky, Phys.Rept. **132**, 1 (1986).

[13] M. Luscher and P. Weisz, JHEP **09**, 010 (2001), arXiv:hep-lat/0108014.

[14] E. H. Fradkin and S. H. Shenker, Phys.Rev. **D19**, 3682 (1979).

[15] K. Osterwalder and E. Seiler, Annals Phys. **110**, 440 (1978).

[16] C. Bonati, G. Cossu, M. D'Elia, and A. Di Giacomo, Nucl.Phys. **B828**, 390 (2010), arXiv:0911.1721.

[17] C. Gattringer and C. B. Lang, Lect.Notes Phys. **788**, 1 (2010).